Chemical Engineering Journal 419 (2021) 129669

Contents lists available at ScienceDirect

Chemical Engineering Journal

journal homepage: www.elsevier.com/locate/cej

Effective removal of hydrogen sulfide using Mn-based recovered oxides from recycled batteries

M. Maroño [a,*], I. Ortiz [a], J.M. Sánchez [a], L. Alcaraz [b], F.J. Alguacil [b], F.A. López [b]

[a] CIEMAT, Sustainable Thermochemical Valorization Unit, Energy Department, Spain
[b] National Center for Metallurgical Research (CENIM-CSIC), Spain

ARTICLE INFO

Keywords:
H_2S removal
Mn-based sorbents
Syngas desulphurization

ABSTRACT

The use of clean and environmentally friendly renewable energy as well as the minimization of waste disposal are fundamental aspects to be considered nowadays in a circular economy approach. In this way, the development of efficient systems for sulfur removal in biomass and waste gasification is of key relevance and the use of recycled materials will provide an opportunity to combine the reduction of waste's production and the application of circular economy principles.

Sorbents from waste powder of recycled batteries have been prepared at laboratory scale. Subsequently, their potential application to syngas cleaning is evaluated specifically for H_2S removal. Lab-scale tests at 400°C, 10 bar and space velocity of 3500 h^{-1} were carried out using first a simplified gas mixture of 0.9% H_2S in N_2 and then a more complex one consisting of 20% H_2, 40% CO and 0.45% H_2S/N_2 to investigate the effect of reducing components, CO and H_2 co-existing with H_2S in any syngas. Sorbent utilization values as high as 80% (w/w, %) were obtained when tested under realistic syngas composition. XRF, XRD, XPS, TEM and textural characterization results of fresh and sulfided samples showed that those materials with higher Mn contents showed higher H_2S removal capacity although the Mn/Zn ratio demonstrated to play a crucial role in their selectivity to form sulfides. Additionally, plausible mechanisms for H_2S removal are discussed where the influence of composition, structure and morphology of the recovered binary metal oxides on sulfur removal efficiency is analysed.

1. Introduction

Removal of reduced sulfur species in gasification processes has been an issue since the 90s. Then, it was mainly associated to coal gasification and to comply with the environmental emission limits associated to syngas combustion in boilers, gas engines and turbines and to prevent corrosion. More recently the focus is on comprehensive sulfur removal in biomass and waste gasification due to the role of syngas and biogas as sources of biofuels. Sulfur removal is now related to preventing poisoning of sulfur sensitive catalysts when upgrading syngas or biogas to biomethane [1]. Particularly, for syngas, technologies relying on regenerable sorbents working in the 300–500°C temperature range are desirable for better process integration [2,3].

Many different solid materials have been tested for H_2S removal such as zeolites [4], activated carbons [5], iron-based materials [6] and different oxides [7]. It is widely reported that zinc oxide and its derivatives are highly effective sorbents for hydrogen sulfide removal, with the ability to reduce hydrogen sulfide concentration to ppmv levels. According to the early study of Westmoreland et al. [8], from the thermodynamic point of view, there are a huge number of potential candidates for high-temperature H_2S removal, among which zinc, nickel and manganese oxides are listed. Zinc oxide is usually the preferred choice based on thermodynamic consideration that indicate very low levels of H_2S, in equilibrium with ZnO, ZnS an H_2O vapor. For example, experimental results at pilot scale proved the sulfur uptake capacity (removal of H_2S) of commercial zinc-oxide based sorbents (Z-Sorb™) at high temperature (300–600 °C) and over a wide pressure range (1–20 bar) [9].

However, it is also known that under a reducing environment, zinc oxide tends to be reduced to elemental zinc [10], reducing its desulfurization capacity. In an effort to solve this limitation, a positive effect of the presence of manganese was observed by Ko et al. who pointed out that manganese oxide can inhibit the vaporization of Zn in reduced atmospheres, and also improve the sulfur capacity of the sorbent [11]. Therefore, Mn-based oxide sorbents attracted the attention of different research groups and significative work can be found in literature on the

* Corresponding author.
E-mail address: marta.marono@ciemat.es (M. Maroño).

https://doi.org/10.1016/j.cej.2021.129669
Received 14 December 2020; Received in revised form 29 March 2021; Accepted 1 April 2021
Available online 8 April 2021

advantages of using Mn oxides for desulfurization processes under aqueous solutions [12,13] or gas flows [14].

The performance of Mn containing sorbents has been extensively investigated, using directly the oxides in form of MnO_x [15], dispersed on different supports including Al_2O_3 and zeolites [16], CeO_2, ZrO_2 and TiO_2 [17] or in the form of mixed metal oxides [18,19].

Studies on hot desulfurization of gases with manganese oxide pellets are reported as early as in 1979. Turkdogan et al. [20] conducted their studies on a pyrolusite ore (MnO_2) which contained 63% Mn (primarily as Mn_3O_4) upon calcination in air. Several years later, supported by the U.S. Department of Energy, DOE, an extensive research on desulfurization of hot coal-derived fuel gases with manganese-based sorbents was carried out by the Morgantown Energy Technology Center, METC, from 1992 to 1997. Manganese oxide is singled out as a good candidate sorbent, capable of being used under a wide temperature range to reduce sulfur concentration in the fuel gas [21]. Moanda ore (77% MnO_2, 3.36% MnO, 6% Al_2O_3, 2.81% Fe, 2.56% SiO_2, and 5.16% H_2O bound) and $MnCO_3$ were shown to hold promise of being affordable, inexpensive sulfur sorbents. They proved successful in reducing the H_2S concentration to <150 ppmv in sulfidation tests using 3% H_2S/H_2 at 700–1000 °C [22]. In subsequent studies expanded to fixed bed testing using a simulated Tampella U Gas (13% H_2, 24% CO, 5% CO_2, 5% H_2O, 3% H_2S, 50% N_2) Ben-Slimane et al. 1995 found that a steady state value 222.5 ppmv was reached, close to that of the MnO/MnS equilibrium, 256 ppmv. In addition, the extent of desulfurization with the Mn-based sorbent was dependent on the water vapor content of the feed gas, that is, lower water vapor content resulted in higher levels of sulfur removal. Cheah et al. [23] did a thorough review on mid- to high-temperature sulfur sorbents for desulfurization of biomass- and coal-derived syngas. In their study, several types of sorbents based on zinc, copper, iron, calcium, manganese and ceria are compared. Manganese-based sorbent showed advantages and disadvantages. In a reducing gas environment, manganese oxides of higher oxidation states are likely reduced to MnO. This is stable and does not decompose to elemental manganese readily in reducing gas environment. Conversely, the thermodynamics of MnO sulfidation is not as favorable as that of zinc oxide or copper oxide.

The use of mixed metal oxides for desulfurization processes have awaked the interest of many researchers because they combine the advantages of the single oxides and the interactions between the different metals can improve the performance of the sorbents and their regeneration conditions. Thus, Girard et al. [3] studied two composites oxides – a single oxides mixture (ZnO and MoO_3) and a mixed oxide ($ZnMoO_4$) for the desulfurization of synthesis gas. They found that regeneration temperatures of binary metal oxides were 250 °C and 300 °C lower than the regeneration temperature of a pure ZnS. Beneficial effects of binary metal oxides have been also reported by several authors during the last decades regarding the role of different metals in desulfurization processes. For example, Polychronopoulouet al. [24] studied various Zn–Ti-based mixed metal oxides and found that the use of manganese (Mn), cupper (Cu), or molybdenum (Mo) in the Zn–Ti–O matrix leads to improved H_2S uptake compared to Zn–Ti–O alone. Shah, who evaluated various Fe-Zn–Ti-based mixed metal oxides, reported the same effect. In his study, he concluded that the addition/incorporation of manganese (Mn) in the Fe-Zn–Ti–O matrix enhances H_2S uptake compared to Zn–Ti–O alone [25]. Other authors studied the performance of $ZnMn_2O_4$ for high temperature H_2S removal from hot coal gas, on direct synthesised $ZnMn_2O_4$ rods [26] or supported on SiO_2 [19].

Although specific mechanisms are not clearly known yet, factors such as the intrinsic oxidative nature of Mn oxides [27,28] or to the reduced crystallinity of binary metal oxides have been reported as critical. Those properties, which can promote the creation of vacancies in the lattice of the solids enhancing the capture process [29] have been suggested to explain the improved H_2S removal capacity observed when Mn species are included in the sorbents.

However, despite the efforts of many authors studying different types of oxides and binary metal oxides containing Mn for the removal of contaminants, the mechanisms, and the influence of the presence of Mn in the removal process are still unclear and require further research.

Spent batteries usually contain heavy and/or transition metals that negatively affect both the environment and human health if they are not properly treated. Therefore, the recycling of spent batteries is undoubtedly an attractive option for the minimization of wastes and application of circular economy principles [30]. The search for novel uses for recycled metal oxides is supported by the rapid technological development of these types of batteries and their use in multiple energy applications, which has caused the generation of a great amount of this type of waste that needs to be disposed [31].

Recovered Zn and Mn ferrite binary metal oxides obtained from recycled batteries have been successfully tested as nano-adsorbents for hazardous metals removal in aqueous phase (As, Cd, Pb) [31] but to the best of the authors knowledge no application of these type of materials to sulfur removal sorbents in gasification gases has been published yet. Consequently, in this work different manganese-zinc and zinc binary metal oxides, recovered from spent alkaline batteries [32,33], have been studied as sorbents for the removal of sulfur in gasification gases at intermediate temperatures (T = 400 °C).

A series of $Zn_xMn_{3-x}O_4$ and ZnO materials were obtained from spent alkaline batteries using a procedure developed at CSIC [33] and their efficiency for the removal of H_2S in the cleaning and upgrading of biomass/wastes gasification gases at intermediate temperatures (T = 400 °C) is presented in this paper. Based on the acknowledged individual capacity of ZnO and MnO to pick up sulfur, it was expected that the recovered oxides, consisting of complex structures of main phase $Zn_xMn_{3-x}O_4$ would show activity towards the removal of H_2S. Although studies of Mn-containing binary metal oxides for the removal of H_2S can be found in literature, performance is usually investigated at temperatures higher than 600 °C (gasification [34]), or lower than 150 °C (biogas cleaning applications [16]) and no references to materials similar to those investigated in this work were found. The performance of a commercial ZnO sorbent (Z-Sorb III^{TM}) and a MnO-based sorbent have been included in the work for comparison.

Attention has been paid to the influence of sorbent composition/structure and to the role of the presence of Mn in the H_2S removal capacity of the sorbents. X-ray diffraction (XRD), transmission electron microscopy (TEM) and X-ray photoelectron spectroscopy (XPS) of fresh and spent samples have been used to identify main sulfured species formed and mechanisms involved.

2. Materials and experimental methods

2.1. Materials

Five different solid materials, four mixed-oxides and ZnO, recovered from recycled batteries, have been studied to determine their suitability as sulfur removal sorbents applicable to syngas cleaning prior to further conversion into added-value products such as fuels or chemicals. The sorbents studied have the general formula $Zn_xMn_{3-x}O_4$, and have been designated with the nomenclature BMOX where X goes from 1 to 4. The ZnO recovered from spent batteries is designated as ZnO-rec.

The recovered oxides investigated in this work were obtained following a procedure described in detail elsewhere [33]. In brief, the process consists of an acidic leaching of the black mass using a mixture of 250 mL of milliQ water, 250 mL of H_2O_2 (Panreac®) and 500 mL of HCl (Panreac®) at room temperature for 1 h. Each recovered oxide was obtained by modifying the solid/liquid (black mass/acid mixture) ratio in the leaching process. The ratios used were 100 g/L, 200 g/L, 300 g/L, or 400 g/L, and the obtained stoichiometry were $Zn_{0.85}Mn_{2.15}O_4$, $Zn_{0.25}Mn_{2.75}O_4$, $ZnMn_2O_4$, and $Zn_{1.25}Mn_{1.75}O_4$, respectively. Finally, the mixtures were filtered, and the collected liquids were precipitated with NaOH 6 M until pH 12–14 was reached. For the ZnO-rec sample, the leaching of the black mass was performed using a solution of $(NH_4)_2CO_3/NH_3$, to guarantee that Mn does not interfere in the leaching

process, and the obtained precursor was calcined during 5 h at 800 °C [32]. The performance of a commercial sorbent, Z-Sorb-III has been included for comparison. Table 1 shows the composition of the resulting sorbent materials in terms of main components, as determined by the XRF analysis.

In Table 1 it can be observed that the active species for H_2S removal in the recovered materials are Mn and Zn with low Ni contents (<1%), while in Z-Sorb III the most abundant species active for sulfur removal is Zn with Ni contents higher than 7%. Those differences in composition are expected to play a crucial role in the H_2S removal capacity of the materials.

2.2. Characterization of the materials

Fresh and post-reaction samples were characterized by several bulk and surface analysis techniques. X-ray fluorescence (XRF), X-ray diffraction (XRD) and X-ray photoelectron spectroscopy (XPS) provided information on the structure and composition of the materials while transmission electron microscopy (TEM) analysis was used to gather information on the distribution of the active phases on the materials surface and N_2 adsorption isotherms were used to determine the textural properties of fresh and spent materials.

Firstly, the mineralogical composition of the samples was determined by X-ray fluorescence (XRF) using a PANalyticalAxios wavelength dispersive spectrometer (4 kW). For the sample preparation, the corresponding solid powders were pressed in Tables (37 mm diameter) using a Herzog HTP 40 press. The results were quantitatively obtained by a comparison with standards. The structural characterization was carried out by X-ray diffraction (XRD) using a Siemens D5000 diffractometer (Cu Kα radiation). The collected data were refined by the Rietveld method using the version 4.2 of the Rietveld analysis program TOPAS (Bruker ASX).

For analyzing the surface of the sorbents X-ray photoelectron spectroscopy (XPS) was used. Spectra of all samples were recorded using a Fisons MT500 spectrometer equipped with a hemispherical electron analyzer (CLAM2) and a non-monochromatic Mg Kα X-ray source operated at 300 W. Binding energies were calibrated to the C 1s peak at 285.0 eV. The atomic ratios were computed from the peak intensity ratios and reported atomic sensitivity factors.

To analyze the contribution of the different species, the deconvoluted area under each peak was obtained fitting the experimental data to a combination of Lorentzian and Gaussian curves of variable proportions until R-squared values of at least 0.995 were achieved. Surface area and porosity was determined by nitrogen sorption isotherms using an ASAP 2000 equipment. Prior to the analysis all samples were degasified at 90 °C for 10 min followed by a heating step at 300°C for 240 min for the removal of humidity and impurities that could be retained in the pores. Finally, the morphological characterization of the fresh and used samples was carried out by transmission electron microscopy (TEM), using a JEOL JEM 2100 instrument. The samples were dispersed in butanol and the suspensions were deposited onto carbon-coated copper grids. X-ray energy dispersive spectroscopy (XEDS) measurements were carried out using an OXFORD INCA instrument.

Table 1
Elementary composition of the materials studied in this work.

Sample	Mn (%at)	Zn (%at)	Ni (%at)
BMO1	71	13	0.54
BMO2	85	6.1	0.78
BMO3	58	20	0.87
BMO4	42	38.0	0.45
Z-Sorb-III[a]	–	41	7.1

[a] Commercial.

2.3. Experimental procedure

All materials were supplied in powder form. Sorbents were prepared by firstly crushing the powder in an agata mortar and then pelletizing at sizes in the range of 0.5–1 mm using a Specat 15 T manual hydraulic press. Testing of the materials has been carried out in a microactivity-pro lab-scale system, an automatic and computerized laboratory rig used for the study of catalysts and sorbents. It is equipped with three independent mass flow controllers to produce desired gas mixtures. Maximum gas flowrate is 4.5 NL/min of maximum gas flow and the system allows studying reactions at up to 600 °C and 30 bar. The reactor, with an internal diameter of 9.2 mm and 300 mm long, as well as all the tubing and fittings of the rig, are manufactured of Hastelloy C, to avoid corrosion problems due to the presence of H_2S. A more detailed description of the test rig is reported elsewhere [35].

Between 2 and 3 g of each material, once pelletized, were used in the experiments and desulfurization tests were performed at 10 bar and 400 °C, using a feed gas mixture of 0.9% H_2S in N_2 with a space velocity of 3500 h^{-1}. These experimental conditions have been selected as representative of desulfurization of biomass gasification processes based on previous experience of authors with commercial ZnO-based sorbents [9]. The H_2S content was set deliberately high, 9000 ppmv, as compared to the expected value particularly for biomass syngas in order to decrease the amount of time to achieve breakthrough. Desulfurization tests were conducted in fixed bed, downward mode.

Inlet and outlet gas composition were analyzed using a CP4900 Varian gas chromatograph equipped with two columns, a Porapack and a molecular sieve column and with two thermal conductivity detectors.

In order to allow the comparison between all materials studied, theoretical values of Sulfur sorption capacity (S_0) and sorption time (t_0) have been calculated based on sulfidation reaction stoichiometry (reactions (1–3)) and the content of the active elements (Zn, Mn, Ni) of each sorbent:

$$ZnO + H_2S \rightarrow ZnS + H_2O \quad (1)$$

$$NiO + H_2S \rightarrow NiS + H_2O \quad (2)$$

$$MnO + H_2S \rightarrow MnS + H_2O \quad (3)$$

The theoretical H_2S sorption capacity of each material, S_0, is the sum of the contribution of the three individual active species, ZnO, MnO and NiO as expressed by:

$$S0(g) = \text{Msorbent}\ (g)*\left(\frac{\text{ZnO}\ (\%)}{100}\frac{\text{MW}_S}{\text{MW}_{ZnO}} + \frac{MnO(\%)}{100}\frac{MW_S}{MW_{MnO}} + \frac{NiO(\%)}{100}\frac{MW_S}{MW_{NiO}}\right) \quad (4)$$

The actual sulfur captured by the sorbent (St (g)), assuming that all sulfur is retained by the sorbent and no sulfur escapes with the gas leaving the reactor until a given sulfidation time t_s, is calculated by the expression:

$$\text{St}\ (g) = \left[\text{MW}_S \cdot \frac{PF_{gas} y_{H_2S}}{R_g T}\right] \cdot t_s \quad (5)$$

Where:

MW_S is the molecular weight of S, P is the absolute pressure at sulfidation conditions, F_{gas} is the volumetric gas flow rate at process conditions, y_{H2S} represents the inlet H_2S mol fraction, Rg is the universal gas constant and T is the absolute temperature at sufidation conditions.

Theoretical sorption time, t_0, was calculated as the ratio between the theoretical amounts of Sulfur, S, that each material can adsorb (g) based on its composition and the Sulfur mass flow rate used in each experiment (g/min).

$$t_0(\text{min}) = \frac{S0(g)}{\left[MW_S \cdot \frac{PF_{gas} y_{H_2S}}{R_g T}\right]} \quad (6)$$

As can be seen, the theoretical time depends on initial hydrogen sulfide concentration, sulfidation pressure and temperature, as well as on gas flow rate, and it will vary according to experimental conditions. Table 2 summarizes theoretical values of S_0 and t_0 calculated for all material studied in this work.

The theoretical capacity of the manganese-based sorbents prepared from spent batteries compares favorably with Z-SorbIII^{TM} as shown in Table 2. In generating this Table, the overall reactions of the active components with H_2S are considered as represented by Eqs. (1–3).

The experimental procedure used was the same for all samples: the system was pressurized and heated up to operating conditions using N_2 as inert gas. When steady state was reached (400 °C and 10 bar), gas mixture, consisting of a mixture of 0.9% H_2S in N_2 was led to enter the reactor. For the simplified syngas-like stream, a mixture containing 0.9% H_2S/40% CO/20% H_2/balance N_2 was fed. Outlet gas composition was continuously analyzed, including the heating and cooling steps and breakthrough curves were obtained until concentration of H_2S reached around 0.1% v/v in the exit gas stream, defined arbitrarily as the breakthrough. Finally, all samples were characterized after the tests by XRD, XPS and XRF in order to identify main sulfured compounds formed and potential changes in structure of the sorbents during the desulfurization process.

3. Results and discussion

3.1. H_2S sorption capacity

The performance of the sorbents was studied in the packed bed in terms of H_2S breakthrough curves.

In a typical experiment, hydrogen sulfide chemically reacts with the active oxides, namely zinc, manganese and nickel oxide to render the corresponding sulfide. Its concentration in the product gas should be equal to that of equilibrium. After a certain time, it slowly rises until it reaches the inlet value. This curve is called the breakthrough curve. In absence of transport and kinetics limitations, the H_2S elution profile would be a step function with $y = y_{eq}$ at $t < t_0$ and $y = y_0$ at $t > t_0$ where y_{eq} and y_0 are the equilibrium and inlet mole fractions respectively. In the actual case, t_0 is not reached due to transport and kinetics limitation and the ratio t/t_0 represents the fractional conversion of the sorbent and allows a fair comparison of performance. The slope of the breakthrough curve is also indicative of limitations to reaction.

Fig. 1 shows the evolution of normalized (H_2S/H_2S_0) concentration at the reactor outlet with the normalized time t/t_0. i.e. the so-called breakthrough curves for all recovered materials investigated in this work. As can be seen in Fig. 1, for all recovered materials investigated in this work, no H_2S is detected at the exit stream prior to break-through (TCD detection limit is 0.1 ppmv), followed by a sharp increase of the H_2S concentration in the reactor outlet.

As all the experiments were performed under the same operation conditions (10 bar, 400 °C and SV = 3500 h^{-1}), material's composition is expected to play the most critical role in the sulfur retention capacity obtained. According to the results obtained, the order in terms of sulfur removal capacity is: BMO2 > BMO1 > BMO3 > BMO4 which is fully in agreement with the estimated theoretical capacity presented in Table 2.

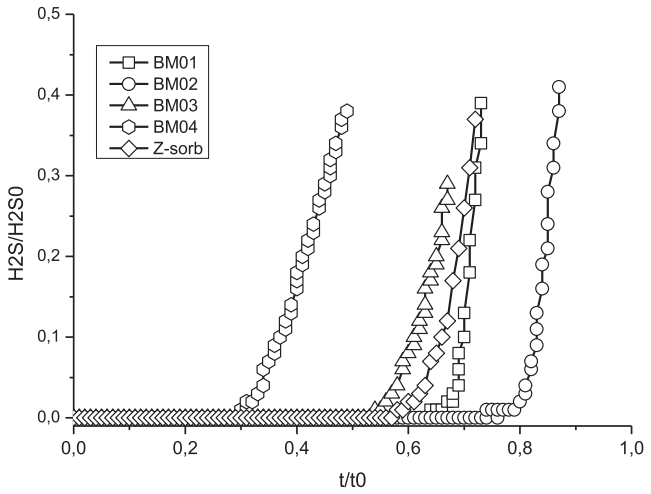

Fig. 1. Breakthrough curves of recovered oxides (10 bar, 400°C and SV = 3500 h^{-1}).

It can be observed that in terms of sulfur retention capacity, two of the manganese-containing sorbents performed better and the other two performed worse than the commercial Z-SorbIII^{TM} sorbent. Moreover, those showing the higher sulfur retention capacity broke through almost vertically, suggesting a fast H_2S capture reaction that stops when sorption centers are no longer available or accessible.

The actual sulfur uptake capacity of the materials is expressed as grams of sulfur adsorbed divided by the mass (g) of sorbent multiplied by 100:

$$S_{uptake\ capacity} = (S_{adsorb}(g)/M_{sorbent}(g))*100 \quad (7)$$

For the evaluation of the performance of the samples in terms of Sulfur removal capacity, the efficiency (%) is used, according to the expression:

$$Efficiency = St/S_0*100 \quad (8)$$

Table 3 summarizes the sulfur uptake capacities calculated until H_2S concentration in the product gas reaches 0.1 %v/v and the efficiency for each material.

Looking at the composition of the materials (see Table 1) it can be highlighted that those samples with lower Zn and higher Mn contents (BMO1 and BMO2) have performed much better than those with higher Zn contents and lower Mn contents. Moreover, there seem to be a straight relationship between the manganese content of the sorbent and its efficiency. Characterization of spent sorbents was performed and results compared to fresh samples in order to investigate sulfidation mechanisms and the role of Mn in the process.

3.2. Characterization results

The composition of the different manganese-containing sorbents

Table 2
Theoretical Sulfur sorption capacity and time of the samples studied.

Sample	Theoretical S sorption capacity, S_0 (% weight)	Theoretical S sorption time, t_0 (min)
BMO1	39	588
BMO2	42	648
BMO3	38	600
BMO4	37	582
Z-Sorb-III[a]	19	282

[a] Commercial.

Table 3
Sulfur uptake capacity and efficiency (w/w %).

Sample	Sulfur uptake capacity St (% weight)	Efficiency (%)
BMO1	28	**65**
BMO2	33	**78**
BMO3	21	56
BMO4	11	31
Z-Sorb III	12	60

studied may have an effect on their sulfur removal capacity and on the sulfidation process.

The characterization of the fresh and used materials investigated in this work showed significant differences in chemical composition, structure and in the sulfur species formed. Three different analysis techniques have been used: XRD provided information on structure, crystallinity and main crystalline phases formed after sulfidation; XPS allowed the identification of different oxidation phases of the sulfured species and finally TEM confirmed the presence of phases, oxides and sulfides. Based on the characterization results an attempt to establish some plausible mechanisms for the removal of H_2S is outlined and discussed in this section.

3.2.1. XRD analysis

Table 4 and Fig. 2 below show the results obtained from the Rietveld refinements of the XRD data for fresh and used samples. XRD analysis shows that, after sulfidation, a loss in crystallinity was observed in all the materials studied, which could be indicative of the formation of amorphous sulfur species. As the sorbents investigated in this work are recovered materials no reference pattern is available for direct comparison and only differences among them and comparison with pure MnO and ZnO oxides can be used.

In the case of the XRD patterns for the fresh samples, the more intense reflexion maxima for all obtained binary oxides samples can be indexed to a tetragonal symmetry, with $I4_1amd$ space group (JCPDS 24–1133) which is consistent with a spinel-type structure, with $Zn_xMn_{3-x}O_4$ general formula [36,37], with the corresponding Miller indices (*hkl*) showed in Fig. 2. Additional peaks, marked in the XRD patterns with crosses (x), are attributed to some impurities related to the sorbent preparation process. In the case of the BM04 sample, reflexion maxima indexed to the ZnO phase were recorded, marked in the XRD patterns with circles (o).

Concerning XRD patterns for the post-reaction samples, $Zn_xMn_{3-x}O_4$ as well as sulfided phases were formed because of the sulfidation process. Clear differences between samples were found: in the case of the BMO2 sample, diffraction peaks, which can be indexed to the α-MnS phase with cubic configuration (JCPDS 06-0518), can be observed. On the contrary, for the BMO1 sample, α-MnS and γ-MnS (JCPDS 40-1289) phases were found. BMO3 and BMO4 samples exhibit diffraction maxima attributable to the γ-MnS phase. An explanation for this is that manganese sulfide can crystallize in three different structures α-, β-, and γ-MnS and at low temperatures (between of 100–400 °C), β-, and γ-MnS are formed, and turned into α-MnS [38]. In addition, an unexpected formation of elemental S was found for BMO1 and BMO2, samples with the highest Mn contents (see Table 1) which resulted in a higher overall sulfur uptake. Finally, XRD pattern for the commercial Z-sorb-III used sample exhibits the presence of hexagonal wurtzite ZnS phase (JCPDS 36-1450). All these observations suggest that increasing amounts of Mn present in the samples result in limited formation of ZnS (or at least it cannot be observed in the XRD pattern).

As expected, main species formed were Zn and Mn sulphides, in the form of ZnS and MnS. However, the analysis also showed the presence of elemental sulfur (S) in the post-reaction samples and it is worth highlighting that this sulfur formation was quantitatively (>8%) identified in those samples showing the highest sulfur removal capacity which were those with higher manganese contents. Formation of elemental sulfur was not expected because all experiments were performed in a non-oxidant atmosphere, as the feed gas mixtures consisted of H_2S/N_2, in absence of oxygen. However, molecular sulfur formation has been recently reported [39] while studying high temperature removal of H_2S using Mn oxides.

Table 4
Rietveld refinement results for fresh and used samples.

Samples	Fresh sample		Used samples	
	Phases	%phases	Phases	%phases
BM01	$Zn_{0.85}Mn_{2.15}O_4$	>95	$Zn_xMn_{3-x}O_4$	504,388
	Impurities	<5	α-MnS	
			γ-MnS	
			S	
BM02	$Zn_{0.25}Mn_{2.75}O_4$	>95	$Zn_xMn_{3-x}O_4$	483,616
	Impurities	<5	α-MnS	
			S	
BM03	$ZnMn_2O_4$	>95	$Zn_xMn_{3-x}O_4$	30
	Impurities	<5	γ-MnS	63
BM04	$Zn_{1.25}Mn_{1.75}0_4ZnO$	721,216	$Zn_xMn_{3-x}O_4$	205,810
	Impurities		γ-MnS	
			ZnO	
Z-sorb-III	–	–	ZnO	29
			ZnS	71

3.2.2. XPS analysis

The results obtained from these analyses provide valuable information about the changes in the oxidation states of the active elements in the materials, during the sulfidation process especially for manganese. Tables 5 and 6 and Fig. 3 summarize XPS results for fresh and sulfided samples. It is widely known that manganese forms stable oxides in different oxidation states (MnO, Mn_2O_3, Mn_3O_4, Mn_5O_8, MnO_2), and may contain labile oxygen in their structures, stored in their crystal lattice. Due to the lability of the interstitial oxygen, Mn can act as a reducing agent ($Mn^{+2} \rightarrow Mn^{+3} + e^- \rightarrow Mn^{+4} + e^-$) or as an oxidant ($Mn^{+4} + e^- \rightarrow Mn^{+3} + e^- \rightarrow Mn^{+2}$) participating in both cases as an active component in the redox system [40]. The activity of manganese oxides depends mainly on the bond strength of oxygen atoms in the outer layer of the surface and this is somehow related to the crystallinity and the thermodynamic stability of the oxides, being lower in the case of less crystalline and less stable oxides (γ-MnO_2 y γ-Mn_2O_3) [29].

The interactions of H_2S with several bulk manganese oxides including MnO, MnO_2, Mn_2O_3 and Mn_3O_4 have been investigated in literature [11,41–43], finding that the production of manganese sulfides with release of water always involve several intermediate transformations where consecutive oxygen-to-sulfur O/S exchanges take place. The mechanisms for those processes remain unclear, though. According also to literature, Mn^{2+} cation can show oxidizing properties when available oxygen in the reaction environment is low [44] and in reducing atmospheres such as H_2S, the following transitions can occur for manganese oxides: $MnO_2 \rightarrow Mn_2O_3 \rightarrow Mn_3O_4 \rightarrow MnO$, being bulk MnO the most active oxide in the reactions with H_2S.

Table 5 summarizes the XPS results for fresh samples where distribution of the different oxidation states in each sample is identified. The obtained bands can be attributed to the bond energies for MnO, Mn_2O_3 and MnO_2 as reported in literature [45,46], showing that manganese is present as Mn(II), Mn(III) and Mn(IV).

In Table 5 it can be observed that both the total amount of manganese and Mn^{+2} phase (which is the manganeses active phase for desulphurization) are higher in samples BMO1 and BMO2. After the sulfidation tests, the presence of different sulphured species, including sulphides (ZnS, MnS, MnS_2) but also sulphates ($MnSO_4$) can be identified. Table 6 summarises the XPS results for the spent samples:

When comparing the Mn 2p3/2 and S2p spectra of spent samples it can be observed that those samples with higher manganese contents (BMO1 and BMO2) showed also a higher sulfates formation and higher sulfur retention capacities. Additionally, elementary sulfur was also detected by XRD in those samples (see Table 4). On the contrary, those samples with lower net Mn contents (BMO3 and BMO4) showed a higher formation of manganese sulfides (MnS/MnS_2) and no S formation.

The presence of both manganese sulfided species MnS and MnS_2 suggested a plausible mechanism to explain the presence of elementary sulfur in some of the samples: the stability diagram for manganese sulfide [47] shows that up to about 625 K (352°C) MnS_2 is the most stable phase. However, at higher temperatures (as those used in our work, 400 °C), manganese is reduced from Mn^{4+} to Mn^{2+} under the formation of sulfur and MnS according to Eq. (9) which is consistent with the XRD

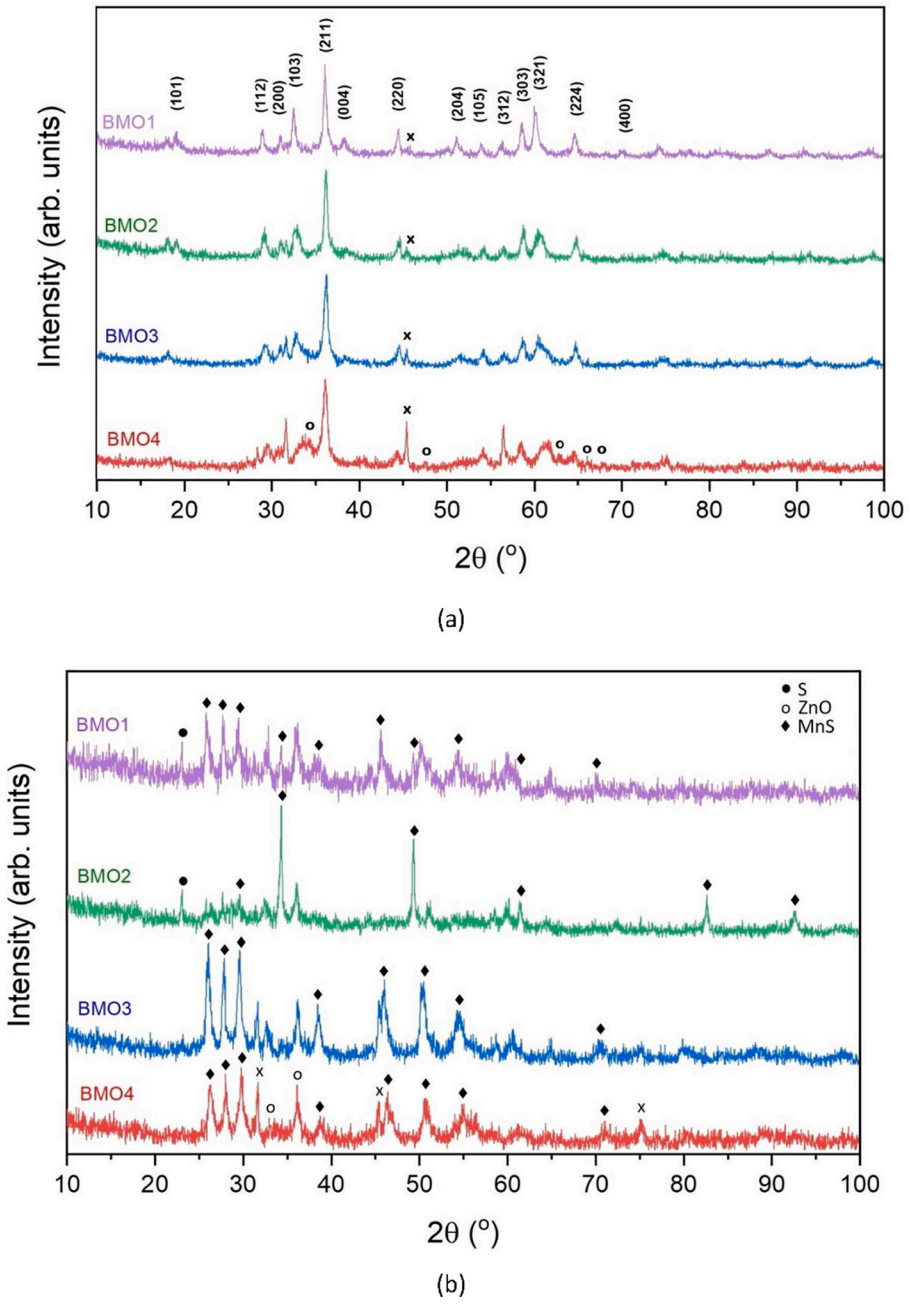

Fig. 2. XRD diffractograms for (a) fresh and (b) used samples.

Table 5
XPS results obtained for the fresh samples (% at).

Sample	% at. Mn (total)	Mn^{2+}	Mn^{3+}	Mn^{4+}
BMO1	26	14	3.0	7.8
BMO2	29	15	4.4	8.5
BMO3	20	6.3	7.3	5.5
BMO4	13	3.4	2.1	7.1

Table 6
XPS results obtained for the used samples (% phases).

Sample	Mn (total)*	S (total)*	ZnS	MnS/MnS_2	$MnSO_4$	Mn
BMO1	24	13	16	51	27	–
BMO2	25	14	25	34	38	–
BMO3	22	16	7.2	78	15	4.8
BMO4	16	14	7.8	82	8.8	–

* % at

and XPS results obtained in this work.

$$MnS_2 = MnS + S \quad (9)$$

Other authors also reported the simultaneous formation of sulfates and elemental S during the oxidation of H_2S with manganese oxides in aqueous phase [12]. Reductive dissolution of Mn (IV) oxides by H_2S gave Mn (II), sulfate, elemental S and low amounts of thiosulfate as products. According to these authors the reaction takes place through the formation of surface complexes Mn (IV)S- and Mn (IV)SH. Further oxidation to S and sulfates takes place following two steps: first the adsorption of H_2S onto Mn surface forming complexes that are oxidized to Mn (II)S via intermediates Mn (III) and then this Mn (II)S formed on the surface follows two competitive reaction pathways towards S (0) or

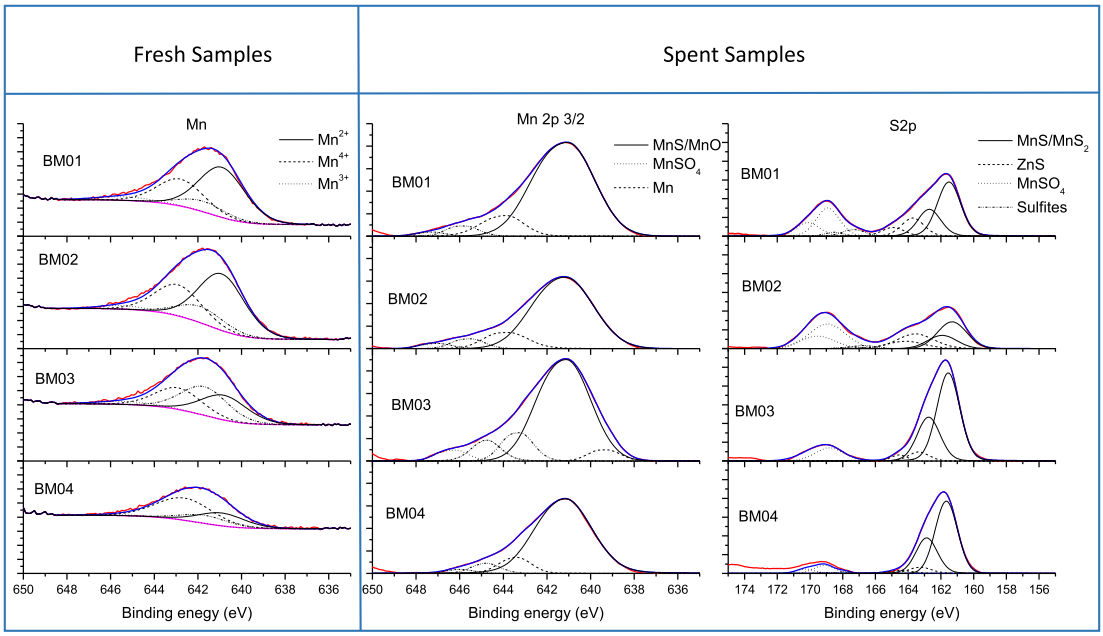

Fig. 3. XPS spectra of fresh (Mn) and spent samples (Mn 2p3/2 and S2p).

$MnSO_4$. No evidence of formation of such intermediates was found in this work. However, the complexity of the structure of the manganese-zinc oxides used for the current study leaves open the possibility of having oxygen atoms available during the desulfurization process. Further in-depth research is needed into the sulfur removal mechanisms when using such complex materials, e.g. by means of more powerful analytical techniques such as operando methodologies wherein the spectroscopic characterization of materials undergoing reaction is coupled simultaneously with measurement of activity.

From the process point of view, however, formation of sulfides is desirable and should be maximized by adjusting operating conditions properly, while sulfates and sulfur formation should be avoided.

3.2.3. TEM analysis

TEM micrographs of fresh samples (Fig. 4) confirmed that $Zn_xMn_{3-x}O_4$ was the main phase, as previously identified by XRD. In all cases, the presence of irregular and heterogeneous particles was observed. It is interesting to highlight that those samples with higher Mn content (i.e. Fig. 4a and b) exhibited larger particles, with near-polyhedral morphology (in some cases, particles with marked sides were observed). However, when the Mn content decreases in the samples, other shapes could be identified as for example nearly-spherical particles in BMO3 (Fig. 4c) or some rod-like structures with elongated particles in the BMO4 sample micrograph (Fig. 4d), which are associated with the presence of ZnO [48,49]. When compared with the corresponding used samples (Fig. 5), an increase in particles agglomeration can be observed and SEM images revealed a general loss of the original shape in all samples. The loss of polyhedral forms of the particles seems indicate the transformation of $Zn_xMn_{3-x}O_4$ spinel-phases into other less crystalline and/or amorphous phases. These results are in good agreement with the XRD section previously described, where the obtained XRD measurements indicate that the sulfidation process leads to a lower crystallinity degree for all analyzed samples, and this is confirmed by TEM micrographs.

The energy dispersive spectra of the fresh and used samples obtained from the TEM-EDS analysis also confirms the changes occurred during the sulfidation process. It can be appreciated that for the fresh samples, main phases contain Mn and Zn characteristic peaks. For the used samples, the S Kα peak was registered in addition. These results clearly confirmed that the H_2S was adsorbed by the samples. Finally, some additional peaks attributable to the carbon-coated copper grids were found.

3.3. Analysis of the effect of the structure in desulfurization performance

The performance and characterization results obtained in this work

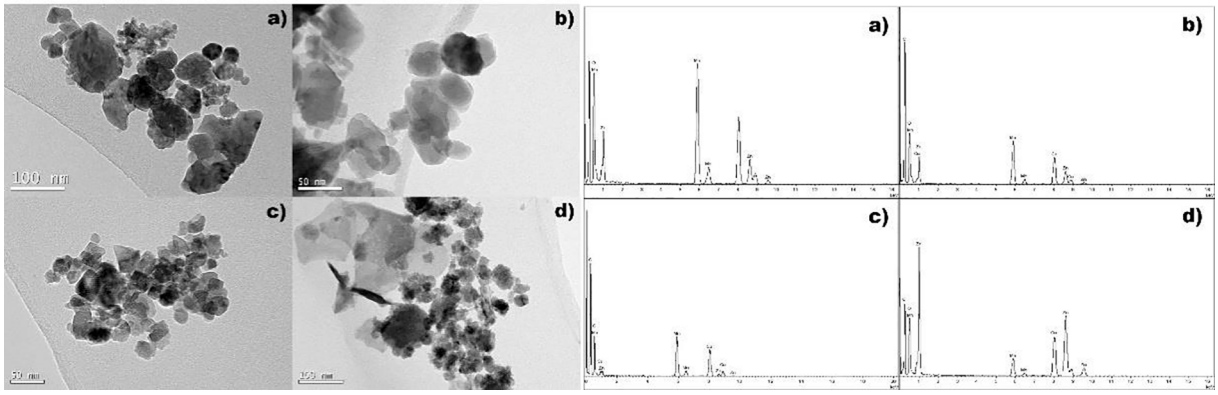

Fig. 4. TEM images for (a) BMO1, (b) BMO2, (c) BMO3 and (d) BMO4 initial samples.

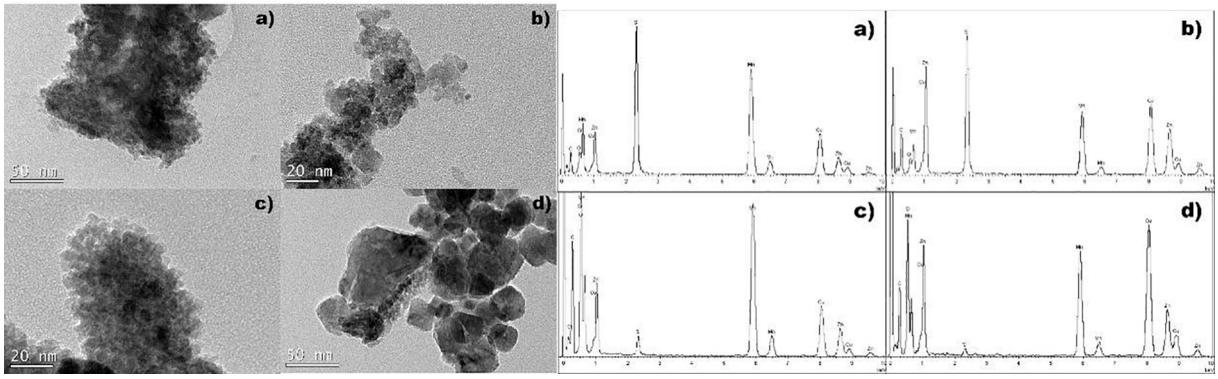

Fig. 5. TEM images for (a) BMO1, (b) BMO2, (c) BMO3 and (d) BMO4 used samples.

have shown that the spinel-based structure and the composition of the mixed-oxide sorbents prepared from the black mass of spent batteries can be playing a crucial role in their desulfurization ability and how the process develops. It is more even so for the manganese species that the sorbents contain.

In order to gather more information on the potential influence of the spinel-based structure on the sulfidation process, some additional tests have been conducted. As the presence of NiO in the recovered materials from recycled batteries is very low (<1% in all cases), we have focused the study on the main components (Zn and Mn). As only ZnO can be separately recovered from recycled batteries with the procedure used in this work, see section 2.1, commercial manganese oxide has been used for the tests.

The performance of the individual oxides (ZnO and MnO) and the corresponding physical blends, BMO1eq and BMO2eq, which mimic the composition of the two best performing recovered materials, BMO1 and BMO2, has been studied. For a fair comparison, experiments have been run under the same operating conditions presented in section 2.3.

Table 7 summarizes the composition of the ZnO-MnO blends investigated in this work for comparison with the recovered mixed-oxide materials. As it can be observed, the relative amounts of ZnO and MnO in the blends are slightly higher than the actual percentages contained in the respective recovered materials.

Although this difference could result in a higher net sulfur removal capacity of the mixtures, for the aim of this work authors decided to use the ZnO/MnO ratio as criteria for preparing the blends of oxides (BMO1eq, BMO2eq) instead of using the same amount of individual oxides present in the recovered materials (BMO1, BMO2) (see Table 7). This approach will provide a more precise analysis of the potential influence of the spinel structure on the Sulfur removal capacity of the materials.

Fig. 6 shows the breakthrough curves for the materials detailed in Table 7. As it can be observed, both recovered materials (BMO1 and BMO2) showed a better performance than their respective equivalent physical blends (BMO1eq and MBO2eq), and much better than the individual oxides ZnO-rec and commercial Mn_3O_4, demonstrating to be more efficient towards Sulfur removal at the experimental conditions tested (400 °C, 10 bar, 0.9% H_2S/N_2).

Table 8 summarizes the results obtained in terms of theoretical capacity (% w/w), actual capacity (% w/w) and efficiency (%). It is observed that the mixed-oxide sorbents BMO1 and BMO2, recovered from spent batteries, showed a slightly lower experimental capacity than their respective blends from the pure components, in accordance to a lower net ZnO and MnO content. Nonetheless, they yielded a higher efficiency than the prepared mixtures. This result suggests that the composition or the spinel-type structure may have a beneficial effect, making the sulfur sorption process more efficient.

In both cases, recovered materials were slightly more efficient (2–4 percentage points higher) than the physical mixtures mimicking their composition. In order to elucidate possible differences in species formed that can justify the higher efficiency, all samples were characterized by XRD, XPS, TEM and porosimetry after the experimental tests. Tables 9 and 10 and Figs. 7–9 show the characterization results.

Characterization of all sulfided samples rend that all materials produced sulfates at some extent when tested under the operating conditions used in this work. In Table 9 it can be seen that formation of

Table 7
Composition of individual oxides and oxides mixtures investigated in this work.

Sample	ZnO (% w/w)	MnO (% w/w)	ZnO/MnO
ZnO-rec	100	–	–
Mn_3O_4	–	100	–
BMO1	15	74	0.20
BMO1eq	17	83	0.20
BMO2	7.2	86	0.08
BMO2eq	7.7	92	0.08

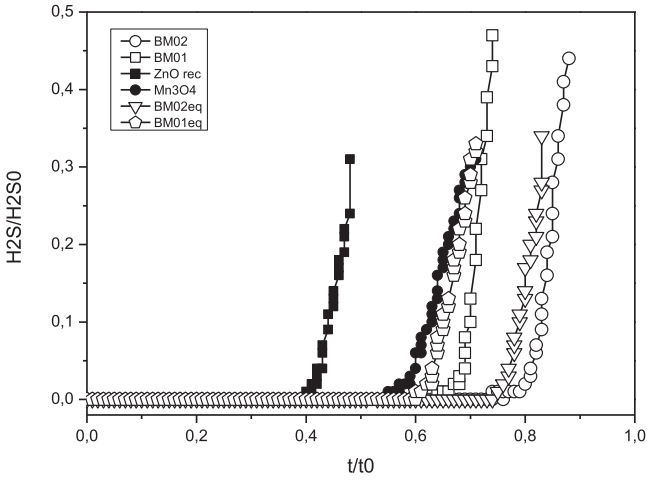

Fig. 6. Breakthrough curves for all materials detailed in Table 7.

Table 8
Performance of ZnO-MnO mixtures.

Sample	Theoretical capacity S_0 (% w/w)	Experimental capacity S (% w/w)	Efficiency (%) S/S_0*100
BMO1	39	26	65
BMO1eq	44	27	62
BMO2	42	33	78
BMO2eq	45	34	76
Mn_3O_4	45	26	56
ZnO-rec	39	16	41

Table 9
XRD and XPS results of sulfided samples.

Samples	XRD		XPS	
	Phases	%phases	Phases	%phases
BMO1	$Zn_xMn_{3-x}O_4$	50	MnS/MnS_2	51
	α-MnS	4	ZnS	17
	γ-MnS	38	$MnSO_4$	27
	S	8		
BMO1eq	$Zn_xMn_{3-x}O_4$	21	MnS/MnS_2	65
	α-MnS	74	ZnS	17
	S	5	$MnSO_4$	19
BMO2	$Zn_xMn_{3-x}O_4$	48	MnS/MnS_2	34
	α-MnS	36	ZnS	25
	S	16	$MnSO_4$	38
BMO2eq	$Zn_xMn_{3-x}O_4$	22	MnS/MnS_2	36
	α-MnS	78	ZnS	42
			$MnSO_4$	22
ZnO-rec	ZnS	72	ZnS	>99
	ZnO-	28		
Mn_3O_4	–	–	MnS/MnS_2	72
			$MnSO_4$	28

Table 10
Porosimetry results of fresh and sulfided samples.

SAMPLES	BET area (m^2/g)	
	Fresh	Sulfided
BMO1	31	7.9
BMO2	41	11
BMO1eq		8.0
BMO2eq		5.0
Mn_3O_4/ZnOcal	8.2–7.4	–

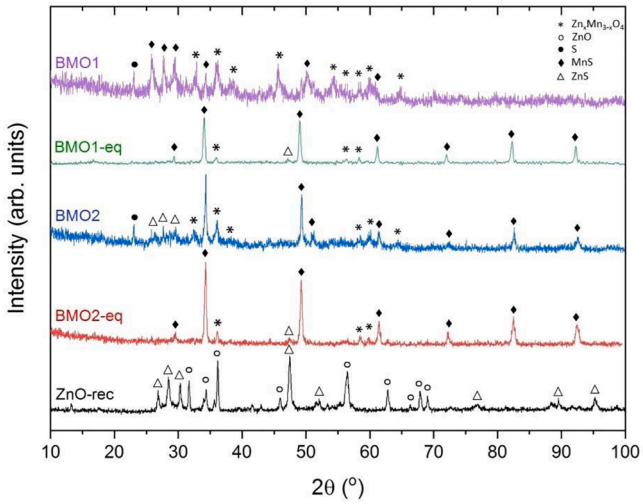

Fig. 7. XRD diffractograms for BMO1, BMO2, BMO1eq, BMO2eq and ZnOrec used samples.

elemental S is lower for the BMOXeq samples (physical blends of Zn and Mn oxides) than for the recovered mixed oxides (16.1% and 15.1% versus 13.3% and 13.7% respectively). Moreover, we found that the ratio Mn/Zn showed a significant influence in the relative formation of sulphides and sulfates. In the case of the blended mixtures mimicking BMO1 and BMO2 (high Mn/Zn ratio) the percentage of manganese sulphides formed was similar for each pair of samples. However, manganese sulfates formation was higher for the recovered samples (BMO1 (26%) and BMO2 (38%)) than for the physically blended samples BMO1eq (18%) and BMO2eq (22%) and zinc sulphides formation was higher for the blended mixtures. This is coherent with the lower elementary S formation and sulfur removal efficiencies obtained.

Textural characterization of fresh and spent samples was performed to elucidate the possible influence of the spinel structure of the recovered materials in the results obtained. Table 10 shows that for the binary mixtures BMO1 and BMO2 sulfidation tests caused a similar decrease of almost 75% of superficial area while for the case of the blended samples important differences were observed between BMO1eq and BMO2eq. From initial similar BET areas of 7–8 m^2/g, sample BMO2eq, with around 15% of zinc oxide and 75% of manganese oxide resulted in a 35% loss of superficial area while sample BMO1eq, with just a 7% of zinc oxide and almost 90% of manganese oxide did not show a significant one. Despite the higher loss in superficial area suffered by the binary oxides, final remaining surface area values were still higher than those remaining in the blended mixtures.

All those results suggested that manganese plays a crucial role in the sulfur removal capacity of these recovered materials and it seems that the ratio Mn/Zn can be a key parameter controlling the formation of sulphides and sulfates. However, as only recovered materials with high Mn/Zn ratio have been studied in detail in this work, further experiments are needed, including the low Mn/Zn ratio materials, in order to elucidate the potential influence of the spinel structure.

3.4. Analysis of the effect of the presence of H_2 and CO in the feed gas

The targeted application of the sorbents investigated in this work is their use as desulfurization agents for syngas streams, whose main components are CO and H_2. Up to now all experiments have been performed using a simplified feed gas mixture of H_2S (0.9% v/v) in N_2. In order to demonstrate their suitability for the proposed application, additional tests were conducted for sample BMO2 using a feed gas composition consisting of 20% H_2, 40% CO and 0.45% H_2S, N_2 balance, identified as $BMO2_{CG}$. Fig. 10 shows the breakthrough curve obtained for both tests.

As Fig. 10 shows, breakthrough curve for $BMO2_{CG}$ was very similar to that obtained when the simplified feed gas was used (BMO2). Despite the higher reducing atmosphere caused by the presence of CO and H_2 in the feed gas, desulfurization efficiencies higher than 80% were reached for sorbent $BMO2_{CG}$.

Spent sample was characterized by XRD and XPS and results showed that a higher selectivity to sulphides was obtained (74%) while sulfates production was reduced (25%) compared to the value obtained for BMO2 when tested under simplified feed gas (38.4%, see Table 9). Main phases identified by XRD in the $BMO2_{CG}$ sulfided sample are manganese sulphides while no elementary sulfur was detected. Those results suggest that the materials investigated in this work are suitable for their use as desulfurization agents in real gasification gases.

4. Conclusions

In this work the sulfur removal capacity of several Zn-Mn binary metal oxides, recovered from waste powder of recycled batteries has been investigated for their potential application to syngas desulfurization at 400°C.

Five different sorbent formulations were prepared from recovered materials, four of them zinc-manganese binary metal oxides and one zinc oxide. Their performance was studied in a lab scale reactor at 400°C, 10 bar and space velocity of 3500 h^{-1} using first a gas mixture of 0.9% H_2S in N_2 and finally under a more realistic syngas composition consisting of a mixture of 20% H_2, 40% CO and 0.45% H_2S/N_2. Commercial zinc and manganese oxide based sorbents have been used for comparison. Characterization of fresh and post-reaction samples were used to understand and suggest a plausible mechanism for the desulfurization process. From the study performed the following conclusions can be drawn:

The most relevant result is that all the materials investigated in this work showed H_2S removal capacity under the operating conditions tested. Among the studied materials, those with higher Mn content

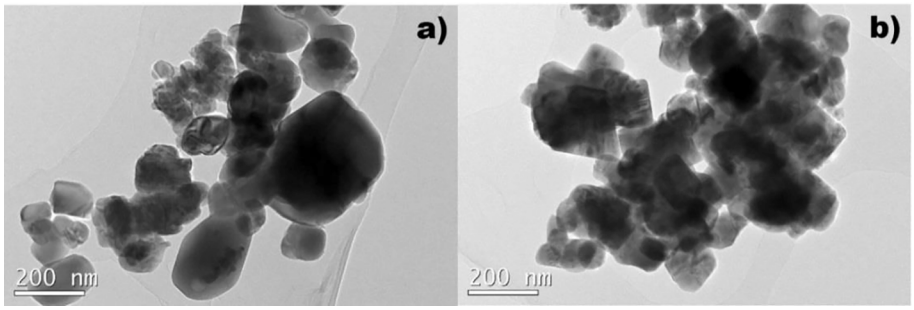

Fig. 8. TEM images for (a) BMO1-eq, (b) BMO2-eq fresh samples.

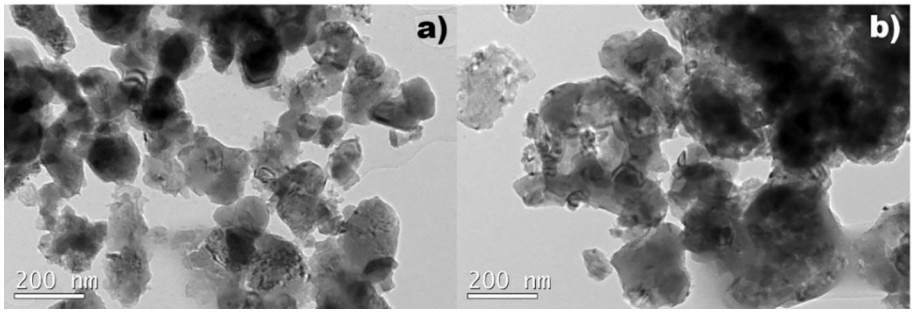

Fig. 9. TEM images for (a) BMO1-eq, (b) BMO2-eq sulfided samples.

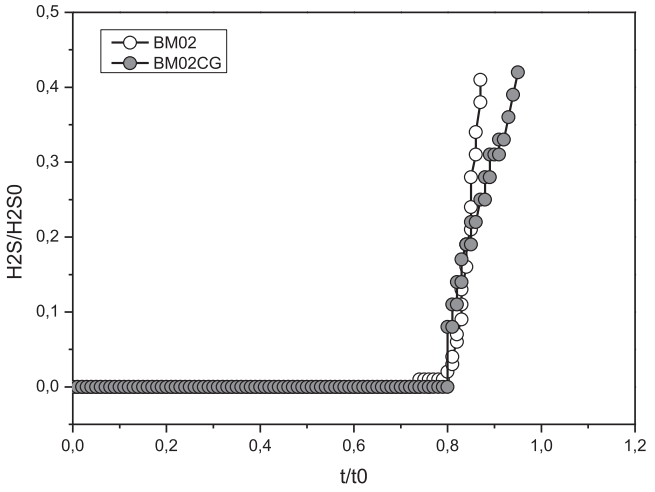

Fig. 10. Breakthrough curves for material BMO2 under simplified (BMO2) and complex ($BMO2_{CG}$) feed gas conditions. P = 10 bar, T = 400°C, SV = 3500 h^{-1}.

showed better H_2S removal capacity, with efficiencies as high as 80%, over performing some of them a commercial ZnO sorbent studied for comparison (Z-Sorb III^{TM})

XRD analysis of the spent samples showed that the $Zn_xMn_{3-x}O_4$ spinel-type structure is not fully destroyed at 400°C. Moreover, high contents of Mn seem to inhibit the formation of ZnS, keeping Zn partially in the sample as ZnO. This can be explained by a rather faster kinetics of MnO compared to ZnO.

In addition to the formation of the corresponding sulfides, formation of sulfates and elemental S took place for some samples. This effect was more intense for those samples with higher Mn contents, which correspondingly showed higher overall H_2S removal capacity. By looking at the XPS results, it seems that the presence of increasing amounts of zinc increases the selectivity of the manganese to form sulfides but reduces the zinc utilization in the samples. Additionally, the formation of elemental S and sulfates seems to be highly dependent on the Mn/Zn ratio, being higher for those samples with a high Mn/Zn ratio.

Finally, the use of a highly reducing atmosphere, consisting of CO, H_2, H_2S/N_2 was found to improve the performance of the materials increasing their selectivity to form sulfides which is a desirable and promising result.

As for future works, it is suggested to investigate the effect of Zn content and Mn/Zn ratio in the sulfur removal capacity of the recovered oxides and to look into the regeneration of the sulfided materials so that they can be used in multiple cycles.

Declaration of Competing Interest

The authors declare that they have no known competing financial interests or personal relationships that could have appeared to influence the work reported in this paper.

Acknowledgements

Authors wish to thank the Spanish Ministry of Science and Innovation for the funds received under the project ECOSGAS [No. ENE2016-75811-R].

References

[1] M. Hervy, D. Pham Minh, C. Gérente, E. Weiss-Hortala, A. Nzihou, A. Villot, L. Le Coq. H2S removal from syngas using wastes pyrolysis chars. Chem. Eng. J. 334. 2018. 217–2189. https://doi.org/https://doi.org/10.1016/j.cej.2017.11.162.

[2] J. Wang, B. Qiu, L. Han, G. Feng, Y. Hu, L. Chang, W. Bao, Effect of precursor and preparation method on manganese based activated carbon sorbents for removing H2S from hot coal gas, J. Hazard. Mater. 213–214 (2012) 184–192, https://doi.org/10.1016/j.jhazmat.2012.01.080.

[3] V. Girard, D. Chiche, A. Baudot, D. Bazer-Bachi, I. Clémençon, F. Moreau, C. Geantet, Innovative low temperature regenerable zinc based mixed oxide sorbents for synthesis gas desulfurization, Fuel 140 (2015) 453–461, https://doi.org/10.1016/j.fuel.2014.09.090.

[4] L. Sigot, G. Ducom, P. Germain, Adsorption of hydrogen sulfide (H2S) on zeolite (Z): Retention mechanism, Chem. Eng. J. 287 (2016) 47–53, https://doi.org/10.1016/j.cej.2015.11.010.

[5] A. Bagreev, H. Rahman, T.J. Bandosz, Thermal regeneration of a spent activated carbon previously used as hydrogen sulfide adsorbent, Carbon 39 (9) (2001) 1319–1326, https://doi.org/10.1016/S0008-6223(00)00266-9.

[6] N. de Arespacochaga, C. Valderrama, C. Mesa, L. Bouchy, J.L. Cortina, Biogas deep clean-up based on adsorption technologies for Solid Oxide Fuel Cell applications, Chem. Eng. J. 255 (2014) 593–603, https://doi.org/10.1016/j.cej.2014.06.072.

[7] D. Liu, W. Zhou, J. Wu, CeO2–MnOx/ZSM-5 sorbents for H2S removal at high temperature, Chem. Eng. J. 284 (2016) 862–871, https://doi.org/10.1016/j.cej.2015.09.028.

[8] P.R. Westmoreland, D.P. Harrison, Evaluation of candidate solids for high-temperature desulfurization of low-Btu gases, Environ. Sci. Technol. 10 (7) (1976) 659–661, https://doi.org/10.1021/es60118a010.

[9] J.M. Sánchez, E. Ruiz, J. Otero, Selective removal of hydrogen sulfide from gaseous streams using a zinc-based sorbent, Ind. Eng. Chem. Res. 44 (2) (2005) 241–249, https://doi.org/10.1021/ie0497902.

[10] N. Abdoulmoumine, S. Adhikari, A. Kulkarni, S. Chattanathan, A review on biomass gasification syngas cleanup, Appl. Energy 155 (2015) 294–307, https://doi.org/10.1016/j.apenergy.2015.05.095.

[11] T.-H. Ko, H. Chu, Y.-J. Liou, A study of Zn-Mn based sorbent for the high-temperature removal of H2S from coal-derived gas, J. Hazard. Mater. 147 (1–2) (2007) 334–341, https://doi.org/10.1016/j.jhazmat.2007.01.018.

[12] J. sdos Santos Afonso, Mechanism of hydrogen Sulfide oxidation by manganese(IV) OXIDE in aqueous solutions, Langmuir 19(23) (2003) 9684-9692. https://doi.org/10.1021/la034016p.

[13] M.A. Kessick, B.M. Thomson, Reactions between manganese dioxide and aqueous sulfide, Environ. Lett. 7 (2) (1974) 163–173, https://doi.org/10.1080/00139307409437394.

[14] Z.F. Zhang, B.S. Liu, F. Wang, W.S. Wang, C. Xia, S. Zheng, R. Amin, Hydrogen sulfide removal from hot coal gas by various mesoporous silica supported Mn2O3 sorbents, Appl. Surf. Sci. 313 (2014) 961–969, https://doi.org/10.1016/j.apsusc.2014.06.116.

[15] L. Alonso, J.M. Palacios, A TEM and XRD Study of the structural changes involved in manganese-based regenerable sorbents for hot coal gas desulfurization, Chem. Mater. 14 (1) (2002) 225–231, https://doi.org/10.1021/cm011130p.

[16] M. Steijns, P. Koopman, B. Nieuwenhuijse, P. Mars, The mechanism of the catalytic oxidation of hydrogen sulfide: III. An electron spin resonance study of the sulfur catalyzed oxidation of hydrogen sulfide, J. Catal. 42 (1) (1976) 96–106, https://doi.org/10.1016/0021-9517(76)90095-6.

[17] S. Chytil, M. Kure, R. Lødeng, E.A. Blekkan, Performance of Mn-based H2S sorbents in dry, reducing atmosphere – Manganese oxide support effects, Fuel 196 (2017) 124–133, https://doi.org/10.1016/j.fuel.2017.01.087.

[18] M. Jie, Z. Yongyan, Z. Yongsheng, G. Ting, F. Huiling, Semi-coke–supported mixed metal oxides for hydrogen sulfide removal at high temperatures, Environ. Eng. Sci. 29 (7) (2011) 611–616, https://doi.org/10.1089/ees.2011.0081.

[19] T.-H. Ko, S. Wang, F.-H. Chang, C.-Y. Chu, Performance of ZnMn2O4/SiO2 sorbent for high temperature H2S removal from hot coal gas, RSC Adv. 7 (57) (2017) 35795–35804, https://doi.org/10.1039/C7RA06785B.

[20] E.T. Turkdogan, R.G. Olsson, Desulfurization of hot reducing gases with manganese oxide pellets, in: A. International (Ed.), Third International Iron and Steel Congress ASM, Materials Park, OH, Park, Ohio, 1979, pp. 277–288.

[21] R. Ben-Slimane, M.T. Hepworth, Desulfurization of hot coal-derived fuel gases with manganese-based regenerable sorbents. 1. Loading (sulfidation) tests, Energy Fuel. 8 (6) (1994) 1175–1183, https://doi.org/10.1021/ef00048a003.

[22] R. Ben-Slimane, M.T. Hepworth, Desulfurization of hot coal-derived fuel gases with manganese-based regenerable sorbents. 3. Fixed-bed testing, Energy Fuel. 9 (2) (1995) 372–378, https://doi.org/10.1021/ef00050a024.

[23] S. Cheah, D.L. Carpenter, K.A. Magrini-Bair, Review of mid- to high-temperature sulfur sorbents for desulfurization of biomass- and coal-derived syngas, Energy Fuel 23 (11) (2009) 5291–5307, https://doi.org/10.1021/ef900714q.

[24] K. Polychronopoulou, J.L.G. Fierro, A.M. Efstathiou, Novel Zn–Ti-based mixed metal oxides for low-temperature adsorption of H2S from industrial gas streams, Appl. Catal. B 57 (2) (2005) 125–137, https://doi.org/10.1016/j.apcatb.2004.10.017.

[25] M.S. Shah, M. Tsapatsis, J.I. Siepmann, Hydrogen sulfide capture: from absorption in polar liquids to oxide, zeolite, and metal-organic framework adsorbents and membranes, Chem. Rev. 117 (14) (2017) 9755–9803, https://doi.org/10.1021/acs.chemrev.7b00095.

[26] P. Zhang, X. Li, Q. Zhao, S. Liu, Synthesis and optical property of one-dimensional spinel ZnMn2O4 nanorods, Nanoscale Res. Lett. 6 (1) (2011) 323, https://doi.org/10.1186/1556-276X-6-323.

[27] A. Schippers, B.B. Jørgensen, Oxidation of pyrite and iron sulfide by manganese dioxide in marine sediments, Geochim. Cosmochim. Acta 65 (6) (2001) 915–922, https://doi.org/10.1016/S0016-7037(00)00589-5.

[28] R.M. Akhmadullin, D.N. Bui, A.G. Akhmadullina, Y.D. Samuilov, Catalytic activity of manganese and copper oxides in the oxidation of sulfur compounds, Kinet. Catal. 54 (3) (2013) 334–337, https://doi.org/10.1134/S0023158413030014.

[29] D. Van de Kleut, On the Preparation and Properties of Manganese Oxide Based Combustion Catalysts, University of Ultrecht, The Netherlands, 1994.

[30] T. Buzatu, G. Popescu, I. Birloaga, S. Săceanu, Study concerning the recovery of zinc and manganese from spent batteries by hydrometallurgical processes, Waste Manage. 33 (3) (2013) 699–705, https://doi.org/10.1016/j.wasman.2012.10.005.

[31] V.J. Inglezakis, K. Moustakas, Household hazardous waste management: A review, J. Environ. Manage. 150 (2015) 310–321, https://doi.org/10.1016/j.jenvman.2014.11.021.

[32] Félix.A. López, T. Cebriano, I. García-Díaz, P. Fernández, O. Rodríguez, A. López. Fernández, Synthesis and microstructural properties of zinc oxide nanoparticles prepared by selective leaching of zinc from spent alkaline batteries using ammoniacal ammonium carbonate, J. Clean. Prod. 148 (2017) 795–803, https://doi.org/10.1016/j.jclepro.2017.02.031.

[33] L.A. Romo, A. López-Fernández, I. García-Díaz, P. Fernández, A. Urbieta, Félix. A. López, From spent alkaline batteries to ZnxMn3−xO4 by a hydrometallurgical route: synthesis and characterization, RSC Adv. 8 (58) (2018) 33496–33505.

[34] P. Caglayan, S. Yasyerli, I. Ar, G. Dogu, T. Dogu, Kinetics of H2S Sorption on Manganese Oxide and Mn-Fe-Cu Mixed Oxide Prepared by the, Complex. Techniq. 4 (1) (2006), https://doi.org/10.2202/1542-6580.1312.

[35] M. Maroño, J.M. Sánchez, E. Ruiz, A. Cabanillas, Study of the Suitability of a Pt-Based Catalyst for the Upgrading of a Biomass Gasification Syngas Stream via the WGS Reaction, Catal. Lett. 126 (3) (2008) 396–406, https://doi.org/10.1007/s10562-008-9644-9.

[36] L. Nádherný, M. Maryško, D. Sedmidubský, C. Martin, Structural and magnetic properties of ZnxMn3−xO4 spinels, J. Magn. Magn. Mater. 413 (2016) 89–96, https://doi.org/10.1016/j.jmmm.2016.04.029.

[37] K. Lilova, G. Sharma, S. Hayun, D.P. Shoemaker, A. Navrotsky, Thermodynamics of ZnxMn3−xO4 and Mg1−zCuzCr2O4 spinel solid solutions, J. Mater. Res. 34 (19) (2019) 3305–3311, https://doi.org/10.1557/jmr.2019.196.

[38] C. Ulutas, O. Erken, M. Gunes, C. Gumus, The effects of substrate on the physical properties of gamma-MnS thin films deposited by chemical bath deposition, Phys. B 588 (2020), 412175, https://doi.org/10.1016/j.physb.2020.412175.

[39] A. Khawaja, High Temperature Removal of H2S by Uusing MnO, Stockholm, Sweden, 2018.

[40] T. Garetto Sodiro, Í. Legorburu Faus, M. Montes Ramírez, Eliminación de emisiones atmosféricas de COVs por catálisis y adsorción, Ciencia y Tecnología para el Desarrollo2008.

[41] J. Więckowska, Catalytic and adsorptive desulphurization of gases, Catal. Today 24 (4) (1995) 405–465, https://doi.org/10.1016/0920-5861(95)00021-7.

[42] L.D. Gasper-Galvin, A.T. Atimtay, R.P. Gupta, Zeolite-Supported Metal Oxide Sorbents for Hot-Gas Desulfurization, Ind. Eng. Chem. Res. 37 (10) (1998) 4157–4166, https://doi.org/10.1021/ie930439i.

[43] Z.R. Ismagilov, R.A. Shkrabina, S.A. Yashnik, N.V. Shikina, I.P. Andrievskaya, S. R. Khairulin, V.A. Ushakov, J.A. Moulijn, I.V. Babich, Supported honeycomb monolith catalysts for high-temperature ammonia decomposition and H2S removal, Catal. Today 69 (1) (2001) 351–356, https://doi.org/10.1016/S0920-5861(01)00389-3.

[44] Ş. Fe, Practical reduction of manganese oxide, J Chem Tech App 1 (1) (2017) 1–2.

[45] O.A. Bulavchenko, Z.S. Vinokurov, T.N. Afonasenko, P.G. Tsyrul'nikov, S. V. Tsybulya, A.A. Saraev, V.V. Kaichev, Reduction of mixed Mn–Zr oxides: in situ XPS and XRD studies, Dalton Trans. 44 (35) (2015) 15499–15507, https://doi.org/10.1039/C5DT01440A.

[46] G.C. Allen, S.J. Harris, J.A. Jutson, J.M. Dyke, A study of a number of mixed transition metal oxide spinels using X-ray photoelectron spectroscopy, Appl. Surf. Sci. 37 (1) (1989) 111–134, https://doi.org/10.1016/0169-4332(89)90977-X.

[47] W.J.W. Bakker, J.C.P. van Rossen, J.M. Mugge, F. Kapteijn, J.A. Moulijn, in: Performance of Manganese-based Sorbents in High-Temperature Coal Gas Desulfurization, Springer, Berlin Heidelberg, Berlin, Heidelberg, 1998, pp. 243–267.

[48] H. Lu, K. Deng, Z. Shi, Q. Liu, G. Zhu, H. Fan, L. Li, Novel ZnO microflowers on nanorod arrays: local dissolution-driven growth and enhanced light harvesting in dye-sensitized solar cells, Nanoscale Res. Lett. 9 (1) (2014) 183, https://doi.org/10.1186/1556-276X-9-183.

[49] I. Musa, N. Qamhieh, S.T. Mahmoud, Synthesis and length dependent photoluminescence property of zinc oxide nanorods, Results Phys. 7 (2017) 3552–3556, https://doi.org/10.1016/j.rinp.2017.09.035.